Characterization of the MMX Rover Locomotion Flight Model for Check-Out and Parameterization

Stefan Barthelmes[1] **Fabian Buse**[1] **Maxime Chalon**[2] **Bastian Deutschmann**[2] **Franz Hacker**[2]
Stefan.Barthelmes@dlr.de

Roman Holderried[2] **Alexander Kolb**[2] **Viktor Langofer**[2] **André Fonseca Prince**[2]

Hans-Jürgen Sedlmayr[2] **Juliane Skibbe**[1] **Bernhard Vodermayer**[2]

[1] German Aerospace Center (DLR)
Institute of System Dynamics and Control
Münchener Str. 20
82234 Weßling

[2] German Aerospace Center (DLR)
Institute of Robotics and Mechatronics
Münchener Str. 20
82234 Weßling

***Abstract*—*IDEFIX* is a four-wheeled 25kg rover that is jointly developed and built by the French Centre National d'Études Spatiales (CNES) and the German Aerospace Center (DLR). It will be brought to the Martian Moon Phobos by the Japan Aerospace Exploration Agency (JAXA) as part of the Martian Moons eXploration (MMX) mission in 2027. IDEFIX's objectives are to scout the surface, demonstrate driving in milli-gravity and perform scientific measurements. To upright after landing on the surface, drive and align the rover to the sun, each wheel is mounted on a leg, which can be rotated full 360° in its respective shoulder joint. In previous publications, the development, flight design and qualification of the locomotion subsystem were presented.**

During the cruise phase there will be several health checks and – once landed on Phobos – the locomotion will be checked-out. To be able to analyze the health state quantitatively and parameterize the system properly, a good characterization of the system is important. The foundation of this characterization are tests and health-checks on the flight model (FM), as well as performance test results on the qualification model (QM). A selection of the post-processing and analysis of this measured data, that was done for the characterization of the Loco FM, is presented in this paper.

TABLE OF CONTENTS

1. INTRODUCTION 1
2. HEALTH CHECK 2
3. POSITION ACCURACY 4
4. OVERLOAD PROTECTION 7
5. RADIATION MONITOR 8
6. SOFTWARE 9
7. CONCLUSION 10
REFERENCES 10
BIOGRAPHY 10

1. INTRODUCTION

The MMX rover IDEFIX's overall mission is described in [1], [2] and its scientific goals in more detail in [3].

The locomotion subsystem (LSS) was developed specifically to the needs of this mission. As shown in Figure 1, this subsystem consists of several mechanics, electronics, thermal and software components.

Besides straight driving on the surface of Phobos, the LSS is required to perform the following tasks: After surviving the impact of the $50\,\mathrm{m}$ free-fall from the MMX spacecraft onto the Phobos surface, the LSS needs to provide uprighting capabilities. To do so, a universal leg- and wheel movement sequence first tumbles IDEFIX onto its belly and subsequently raises the rover body to stand on its four wheels. For a more efficient recharging, the LSS can tilt the rover body and an algorithm under CNES responsibility uses a sun sensor to get to the optimal orientation. When driving, IDEFIX also needs to drive curves and even perform point turns. Lacking dedicated steering actuation, this is achieved with a differential drive, called skid steering or tank drive. To improve the traction in very soft sand and on slopes, an inching mode is implemented in which the front and rear wheels move sequentially while the rover body moves up and down.

The interested reader is referred to the following LSS-related publications: The development and FM design of the entire LSS is presented in detail in [4], [5] and its mechanics in [6]. The planning and results of the LSS qualification campaign are summarized in [7]. Details on all the LSS functions and their kinematic control implementation are presented in [8] and Fault Detection, Isolation and Recovery capabilities in [9].

During the development, but especially in the course of the qualification [7] and acceptance campaigns, a large number of tests has been performed. Health checks of different extent will continue to be performed every 3-6 months during the cruise phase and a comprising check-out will be done once IDEFIX has successfully uprighted itself and recharged its battery on Phobos. For a quick assessment of health check and check-out results and for an initial parameterization of the LSS software, a good characterization of the LSS is crucial. This characterization is done by an in-depth analysis of the measurement data of the aforementioned tests to an extent that goes well beyond what was formally needed for the qualification and acceptance of the LSS.

In this paper, we give examples of how test data is used to characterize the LSS as well as to generate a reference for upcoming health checks and the LSS check-out on Phobos.

979-8-3503-0462-6/24/$31.00 ©2024 IEEE

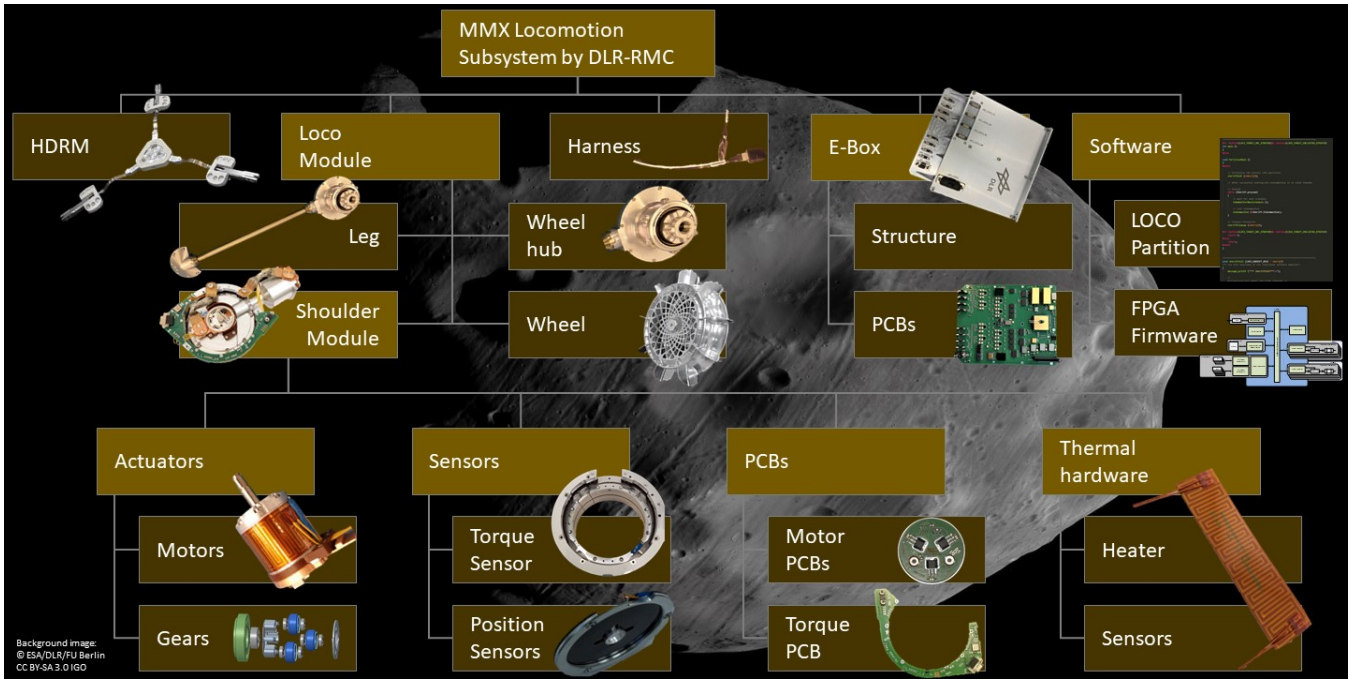

Figure 1: Components of the locomotion subsystem

While the LSS is locked in its HDRMs, only health checks can be performed, which is why this is the only data source during the cruise phase of the mission. The content of the health checks are summarized in Section 2 and some data analysis examples are given. Since IDEFIX has an active chassis, the knowledge of the leg angle is crucial for the mission. Section 3 gives an overview of the drive train accuracy, the used position sensor as well as a simulative analysis of the overall rover pose accuracy. The mechanics of the LSS are designed for the very low Phobos gravity. Although margin is applied, a blockage of a leg or wheel in rock formations or pinching of a small stone between leg/wheel and the rover chassis can lead to damage. Therefore, a blockage detection algorithm is implemented and the measurements that are used to parameterize the algorithm are presented in Section 4. A radiation monitor is assembled in the LSS E-Box. Due to its dissipation and temperature-dependency, it needs to be calibrated for the electrical system at hand. The measurement that is used for that is shown in Section 5. Part of the LSS is the LSS software, which runs on IDEFIX's on-board computer. A characterization of software metrics is presented in Section 6.

2. Health Check

As said in Section 1, the legs and wheels will be locked throughout most of rover AIT, as well as the integration on the spacecraft in Japan and the cruise phase. It is thus important to define a test sequence that confirms the locomotion health as good as possible in this configuration without external motion of the legs or wheels. To that end, the health check (HC) sequence is defined in detail in [7]. It is executed before and after each test campaign and sometimes during the tests in order to detect issues as early as possible and implement corrective methods if required. The full HC consists of the following steps:

- Power-up the E-Box and establish the spacewire link between E-Box and OBC.
- Passive HC: Progressive switch-on of components (e.g. gyroscope, motor inverters, hall sensors, phase current measurement) to test them and locate potential short circuits.
- Active HC: Actuators are moved by 6 increments back and forth to confirm commutation and hall sensor function.
- Power-off

The telemetry collected during the HC is used to establish a baseline and detect deviations. In particular, the following data-sets are of interest:

- Status of the software state-machine and events
- Supply voltages and reference voltages
- Motor position
- Motor current
- Torques
- Leg positions (Potentiometers)
- Temperature sensors
- Accelerometer data
- Gyroscope data

Not all data analysis can be shown in this paper, therefore, only the measurements during the active HC are presented. This check is selected since it is the most important check from a mission perspective. Indeed, its goal is to confirm that the actuators are able to move and that the incremental position sensor of the motors are operating nominally. This is the minimum function needed to deploy the rover on Phobos and orient the solar panels towards the sun. In Figures 2 to 5, different sensor values (line style) are shown for the same test sequence at five different times (colors): *Initial* (blue) is the first test after building and calibrating the FM LSS hardware. This test was performed in February 2022 before the environmental tests of the subsystem acceptance campaign. *Integrated* (orange) was performed almost one year later in January 2023. In between initial and integrated, the LSS has seen its full acceptance test campaign, several shipments as well as the integration in Bremen and Toulouse.

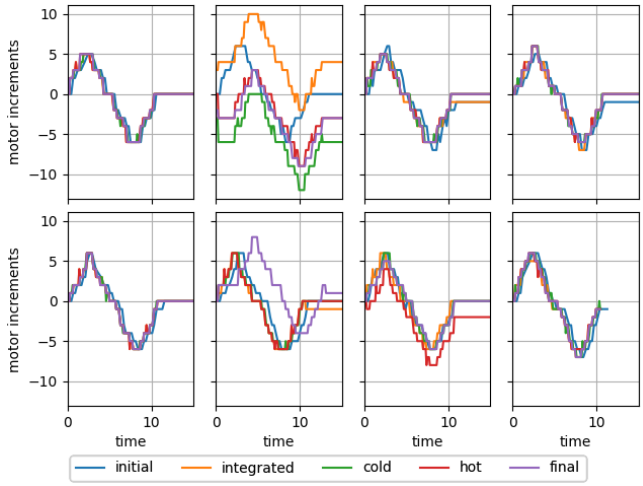

Figure 2: Motor position during active HCs, each actuator is expected to perform a six-steps move. The measurements confirm that all actuators are moving and the hall position sensors are functional.

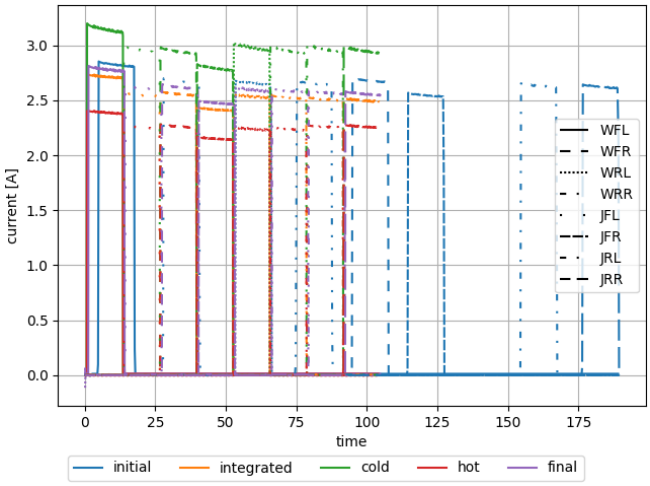

Figure 3: Motor current during active HCs.

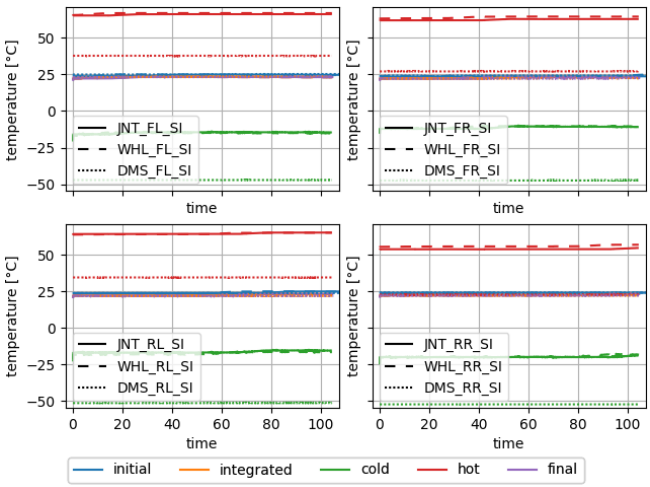

Figure 4: Shoulder temperatures. JNT are the sensors at the leg motor and WHL the wheel motor. DMS is at the torque sensor, which is thermally between the actively heated regime and the cold connection to the chassis. The start temperatures of JNT and WHL in the cold test confirms that the active heating is working.

This is the first test with the LSS fully assembled in the IDEFIX rover. *Cold* (green) and *hot* (red) are performed during the cold and hot phase of the rover thermal cycling test (TCT) campaign, respectively. *Final* (purple) is after full rover TCT and shaker tests have been completed.

During the active HC check, the eight motors are moved one after the other by +/-6 increments, which corresponds to a rotation of the output of only $0.024°$ to not stress the locking mechanism of the LSS or the chassis structure. This movement is commanded in the feed-forward mode, thus the increments are not feed-back controlled. In Figure 2, this open-loop movement is shown as measured by the hall effect sensors for all eight motors. As long as the desired trajectory is achieved with +/-2 increments for each movement, the motors and hall effect sensors are functioning nominally. This is the case in all runs. Note that the subplots in the second column show an offset for some of the tests. This is an expected behavior due to the random start angle of the rotor with respect to the first commutation pattern. The deviation within the +/-2 increment tolerance differs from run to run and spikes, where the position goes to a new increment value and then decreases by one increment right away, results from a settling of the rotor and is expected.

For a more in-depth analysis of the motor health, the motor currents during the active HC are shown in Figure 3. It can be seen that the eight motors are powered one after the other. The test duration of the initial test is longer than the others due to a change in the test script between this first test and the rover AIT HCs. The currents can be compared to each other but also to earlier tests, which gives an indication of changed resistances in the electric circuit, e.g. due to component degradation or connection/harness issues. However, a change in the efficiency – which could indicate mechanical degradation – cannot not be detected from the current measurement due to the feed-forward motor mode. In this mode, the current is set to a fix parameter independent of the required torque. Only very high friction or blockage in an early gear stage or bearing would result in the motor not following the pattern anymore. Increased friction on the other hand will only become visible in the motor current measurements once the LSS is unlocked and larger movements in the feed-back control mode are performed.

The thermal response (cf. Figure 5) is a confirmation that the energy injected in the actuators has the correct amplitude and that the thermal conductivity path has not changed. It clearly shows the temperature increase motor by motor corresponding to the active HC. The temperature levels of the different tests (cf. Figure 4) give a reference of the actual motor temperature and an indication of the proper function of the LSS heaters.

Finally, the torque sensor outputs (cf. Figure 6) demonstrate that the torque sensors are functional. Indeed, although the shoulder rotation during an active HC would only be $0.024°$ for an ideally stiff system, the torque shows a clear pattern. Besides its own functionality, this also indicates that the torque path, i.e. the motors and gear stages, are in good health. Of course, a full health analysis of the gears would require a full $360°$ rotation and is thus not possible during

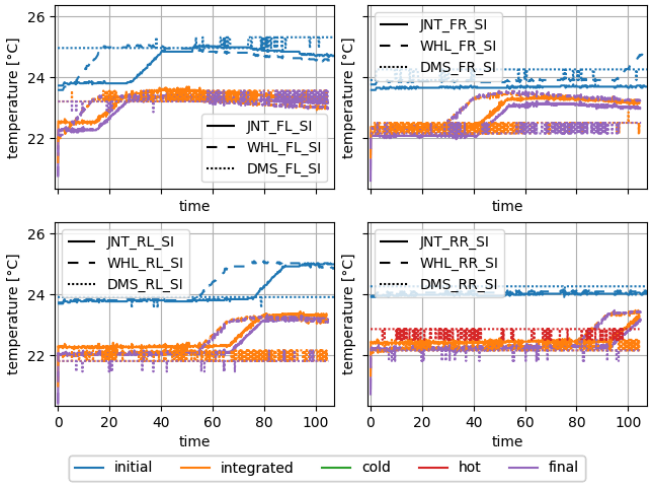

Figure 5: Shoulder temperatures (zoomed to ambient). A temperature step can be observed for each motor during its active HC and indicates that currents and thermal conduction are nominal.

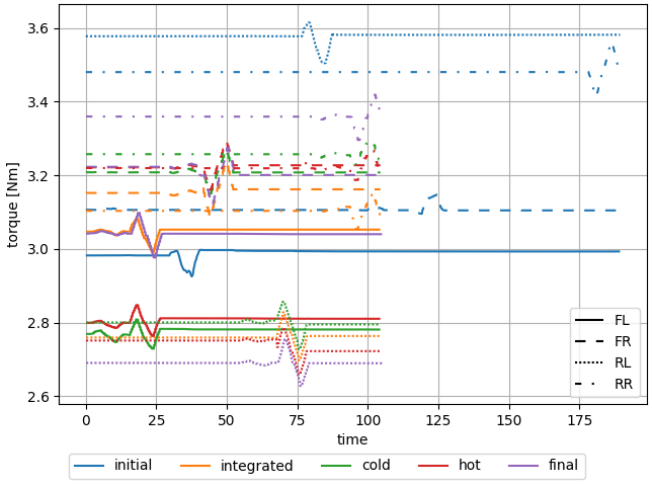

Figure 6: Joint torque measurements. The torque sensor response clearly indicates that the gear train is functional and mirrors the actuator active HCs.

cruise. However, since potential damage in the gears is likely to happen around the locked position, this test is already quite conclusive. Note that the absolute torque values are not relevant since the system is locked and is therefore under a pre-load. In particular, a big difference in the absolute values between the initial test, where the legs and wheels were not yet assembled and not locked in the HDRMs, and all subsequent tests on the assembled rover can be observed. However, the relative changes clearly mirror the active HC of the actuators in all test runs.

3. Position Accuracy

The leg angle knowledge is crucial for reaching a coordinated pose, be it for driving, sun alignment or even the very first phase – the uprighting. Since this is such a mission critical value, the accuracy of this angular position is elaborated in this section. Two sensors yield information about the leg

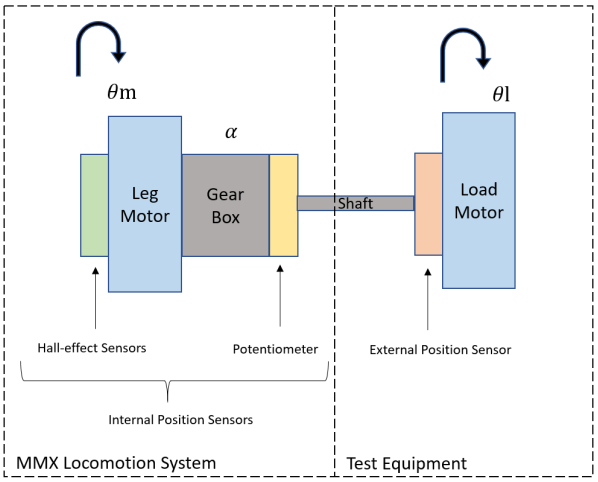

Figure 7: Backlash diagram for performance test setup.

angle: (1) the hall effect sensors that are used to get an accurate relative position of the motor and (2) the potentiometer. To relate these two sources of position knowledge, the overall mechanical drive train layout is first briefly explained in the next subsection and backlash and stiffness are characterized and quantified. These two properties allow to relate the motor-side relative position measurement and the shoulder-side potentiometer. After that, the accuracy of the potentiometer is analyzed. Finally, the simulative approach to compute the overall rover pose accuracy from the position accuracy of the shoulders is explained and results are shown.

Drive train layout, backlash and stiffness

Figure 7 presents a diagram which illustrates the LSS sensor position in the drive train and the external performance test equipment. Other than depicted in the figure, the leg motor movement is not ideally transferred to the load side. There are two factors influencing the relation of leg motor to shaft position: backlash and compliance of the system (i.e. stiffness). The play under no-load operation is defined as backlash (α). It is represented in (Figure 8) by the two dashed red lines. It was calculated as the difference between the motor hall encoder position and the reference position sensor reading at no load operation. Even though no external load is applied for the backlash quantification, a torque of up to $0.5\,\mathrm{N\,m}$ can be seen in the backlash regime due to the friction of the shoulder sealing. The backlash is caused by the gear tooth traveling in the clearance space between two successive opposite teeth until it engages with the load. This happens when changing direction of rotation.

The stiffness (K) of the gear box and shaft components adds to this error when a load is applied. It is caused by elastic deformation of the drive train components and can be approximated as the slope above and below the dashed red lines in the chart shown in Figure 8. The higher K is, the steeper the slope and the faster the transmission response rate. This lagged motion transfer is also reflected in the measurement of the LSS-internal position sensors. A position delta between the motor-side position (hall-effect sensor) and shoulder-side position (potentiometer) results. This error must be considered when commanding or measuring the actual position of the rover's wheel or shoulder.

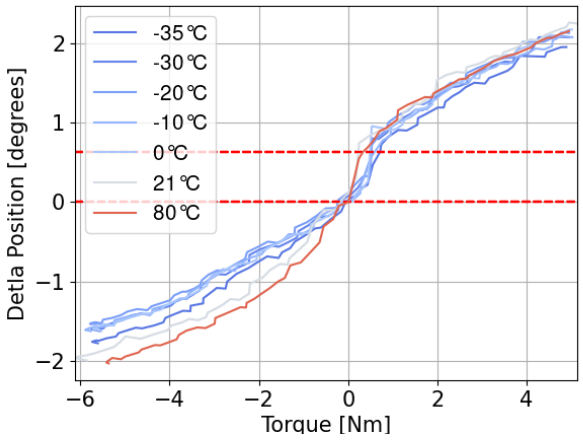

Figure 8: Backlash and stiffness measurement during performance test for different loads at different temperatures. The actuator is not moving, while an external load is allied. The position differences is between the mounting point and the reference sensor.

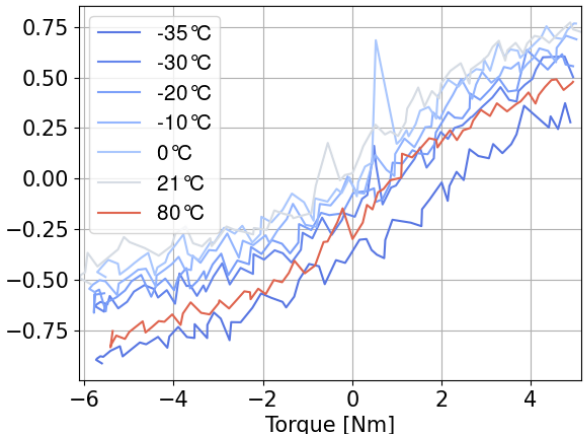

Figure 9: Backlash and stiffness of shoulder structure between potentiometer and reference sensor. This also includes compliance of the actuator housing and the torque sensor

The values for backlash and stiffness were extracted from the performance test data. The mean backlash over the whole temperature range for the shoulder actuator is $0.63°$. A temperature dependency showed to be neglectable in the measurements. The backlash was calculated as the position error between a positive ($0°$ to $700°$) and negative ($700°$ to $0°$) motion under no load.

The load cases were evaluated during a transition from negative maximum load to positive maximum load with no motion of the actuators. In Figures 8 and 9, the results for the shoulder actuator can be seen. Figure 8 shows the overall position delta between motor-side and shoulder output side over the whole torque range and at different temperatures. The stiffness was calculated in the section of $100\,\%$ and $50\,\%$ of the nominal torque range, i.e. between $2\,\mathrm{N\,m}$ and $4\,\mathrm{N\,m}$. The plots show a slightly increasing stiffness at colder temperatures, however, the effect is not significant. The mean stiffness over the temperature ranges in the positive torque range is $3.6\,\mathrm{Nm/°}$ and $3.15\,\mathrm{Nm/°}$ in negative direction. This difference is most likely caused by the negative to positive load transition during recording. A positive to negative recording was not done, so this could not be validated.

In Figure 9, the position difference between the calibrated potentiometer readings and the reference sensor is plotted. One can notice that there is no dedicated step at the zero crossing. This is due to the fact, that there is no play in the connection of the output flange of the shoulder drive train and the reference sensor. However, it can be seen that the connection is not ideally stiff, leading to a position measurement error, especially under significant load. Since test equipment stiffness is already compensated, the cause for this remaining delta is the shoulder drivetrain design. The potentiometer references to the motor housing and hence only picks up the position error of the gear stages. It does not measure the deformation of the overall shoulder structure and especially of the torque sensor structure that is between the actuator and the bolted connection to the rover chassis. A slight steepness change can be observed around $2\,\mathrm{N\,m}$ where the overload pins start to engage.

Potentiometer accuracy

The potentiometer is used for an absolute measurement of the leg angle and is based on an off-the-shelf component, that has been qualified for usage in extended environmental conditions. The sensor consists is produced by an external supplier of a FR4 substrate on which the resistive tracks are screen-printed and thermally cured in several steps.

Figure 10 shows the dimensioning of the sensor. The outer diameter of $45.4\,\mathrm{mm}$ as well as the inner and outer contour have been designed to precisely fit into the LSS shoulder. The sensor is fixed to the stationary part of the joint by riveting and connected to the joint's sensor board by space qualified cabling. On the rotary part, a specially designed carrier for the tiny poti-wiper is installed. To prolong lifetime of the wiper as well as to enable rotations of more than 360°, the surface at the transition between the track-leads in the so called "dead-zone" is smoothed using a printed filler. The accuracy of the potentiometer is theoretically unlimited as there are no discrete gradations in the resistive tracks. Their print is continuous and resistive changes occur on a molecular scale. To this end, the accuracy mainly depends on the mechanical structure of the joint as well as the signal to noise ratio of the used acquisition circuits. Even the tiny grabber with a material thickness of less then $80\,\mu\mathrm{m}$ will contribute a slight backlash when changing rotational direction.

Calibration and Validation—To relate the analog-digital converter (ADC) readings of the potentiometer to a physical turn of the leg, a look-up-table is applied in the on-board LSS software. This look-up table is generated in a calibration procedure during the final flight model integration using the motor position encoder readings. The left of Figure 11 depicts the raw potentiometer measurements (poti) and the hall effect sensor based motor position (theta), whereas the right depicts the resulting lookup table which consists of a piecewise linear interpolation of poti-measurements with 17 support points of theta.

For a validation, an external reference position sensor is needed. Since such a sensor is only available in the performance test setup (see Figure 7) and the FM hardware is not performance tested, the approach itself is validated on the

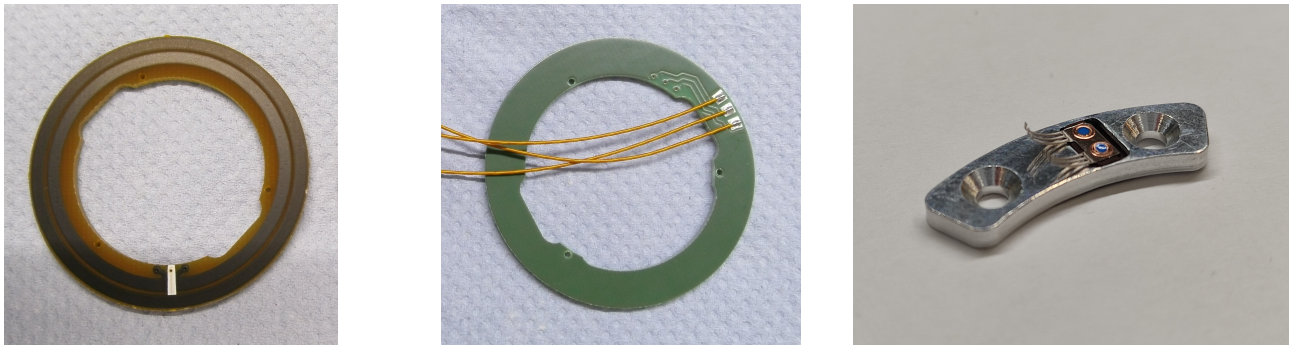

Figure 10: Potentiometer Sensor with tracks (left), backside with leads (mid) and wiper on its carrier (right)

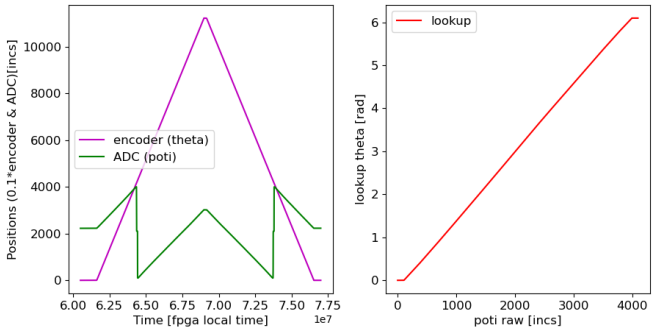

Figure 11: Left: Motor encoder (magenta) and potentiometer (green) readings during a forward and backward 400deg turn of the whole drivetrain. Right: Calibrated lookup table to relate the ADC incremental values of the potentiometer to a rotational motion of the motor.

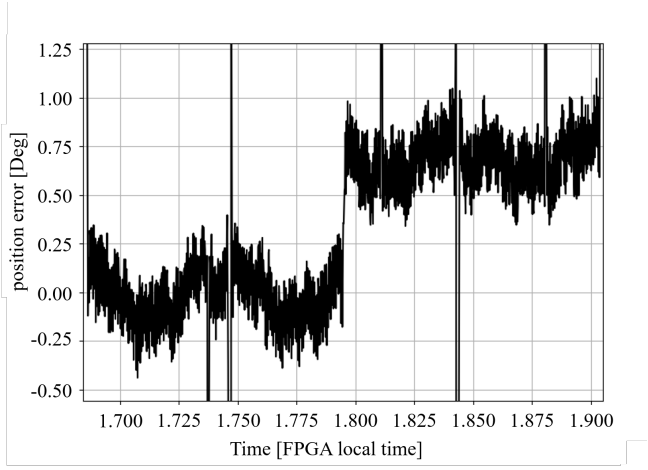

Figure 12: Time based error of the calibrated potentiometer readings and the measurements of the external reference encoder. The vertical jump at 1.8 can be related to the reversal point of the recorded motion and originates from the backlash of the drivetrain and backlash in the sensor principle and can be approximated by $0.6°$.

QM. Using the look-up table, the position error is calculated as the delta between the calibrated potentiometer readings and the external reference encoder. In Figure 12 this error of the predicted leg position can be seen: A maximum of $1.25°$ for a motion of two full motor turns in both directions.

To evaluate the degradation of the potentiometer readings over the FM acceptance campaign, the same calibration is used for a large movement test before and one after the acceptance campaign. The calibration table is therein generated using the initial test results from before the acceptance tests. The delta between motor encoder based and calibrated poti based leg position is plotted in Figure 13. The blue line shows the deviation for the initial test, which was used for calibration. It is expected that there is a delta due to the backlash in the drive train between motor encoder and potentiometer that cannot be calibrated. To quantify the degradation, the mean, minimum and maximum error over a full rotation are compared between the initial and following tests (see the green lines in Figure 13). These deviation values are summarized for each of the four shoulder motors in Table 1. Besides the initial test, the test after the subsystem acceptance campaign as well as after integration into the chassis is shown. The rear right leg shows the largest shift by about $0.3°$. Due to the lack of an external reference sensor, it cannot be assessed, if indeed the potentiometer is shifting or if it reflects an actual slight change in the drivetrain characteristics. However, the shifts are rather small and easily within the leg angle knowledge tolerance of $\pm 2.5°$. The calibration will be repeated with the last test on the PFM rover before the LSS is locked to account for all changes thus far.

This analysis therefore serves the purpose to get a feeling of what magnitude of variation is to be expected during launch, cruise and impact.

Rover pose accuracy

The backlash, potentiometer accuracy and stiffness are a LSS-internal performance metric. To assess the performance requirement of the overall rover pose, the aforementioned shoulder-level values need to be kinematically translated into the resulting rover behavior. In particular, the performance in pointing the rover, and thus solar arrays, in a specific direction is critical. Two key metrics characterize this ability. The absolute orientation (AO) error describes the misalignment of the rover normal with an expected normal and the absolute height (AH) error describes the difference between the commanded and resulting chassis height.

A kinematic model of the rover, in combination with a statistical description of the terrain, is used to compute the impact of the various LSS-internal errors onto the rover pose error. In the kinematic model, the LSS-internal errors can be directly applied. The differences between the assumed contact points between the ideal and the model including errors describe the errors only resulting from locomotion. As the wheels of

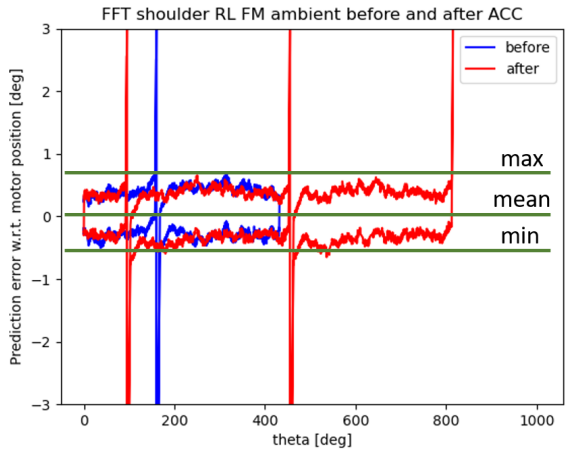

Figure 13: Deviation between calibrated potentiometer readings and the motor encoder. Blue is the error before the acceptance campaign, red is the error after the acceptance campaign.

Table 1: Mean, minimum and maximum prediction error of the calibrated potentiometer readings initially, after subsystem acceptance and after integration into the rover chassis.

error [°]	FL	RL	FR	RR
Initial mean:	0.06	0.1	-0.07	-0.11
max:	0.72	0.7	0.57	0.48
min:	-0.64	-0.51	-0.82	-0.66
after acceptance mean:	0.01	0.05	-0.03	0.19
max:	0.85	0.67	0.61	0.83
min:	-0.94	-0.68	-0.72	-0.46
after integration mean:	-0.1	0.09	-0.04	0.19
max:	0.8	0.66	0.59	0.80
min:	-0.9	-0.69	-0.84	-0.45

the locomotion system generally describe an overdetermined system, one of the four possible contact triangles is randomly picked. The picked contact triangle is then placed on the generated terrain to include errors resulting from the terrain.

Errors like the assembly tolerances were assumed to be uniformly distributed within the possible bounds. As the load due to gravity is smaller than the expected backlash, it is not expected that the side on which the play sits can be predicted. It is more likely that small shifts in terrain consistency lead to a random side of the backlash being favored at each time. Thus, this analysis randomly picks the backlash at either end.

The error sources used in this analysis are:

- Backlash, $[-1.2°, 1.2°]$, which includes some margin compared to the value from Figure 8
- Total error due to manufacturing tolerances, $[-0.13°, 0.13°]$

The resulting distributions are shown in Figure 14 and the resulting 99.78 percentiles are shown in Table 2. Comparing the errors induced by the locomotion system with the errors induced by the expected terrain roughness no significant impact can be observed.

Table 2: Computed three sigma errors for system performance

-	Loco	Terrain	Combined
AO	1.4°	13.5°	13.6°
AH	7 mm	44 mm	45 mm

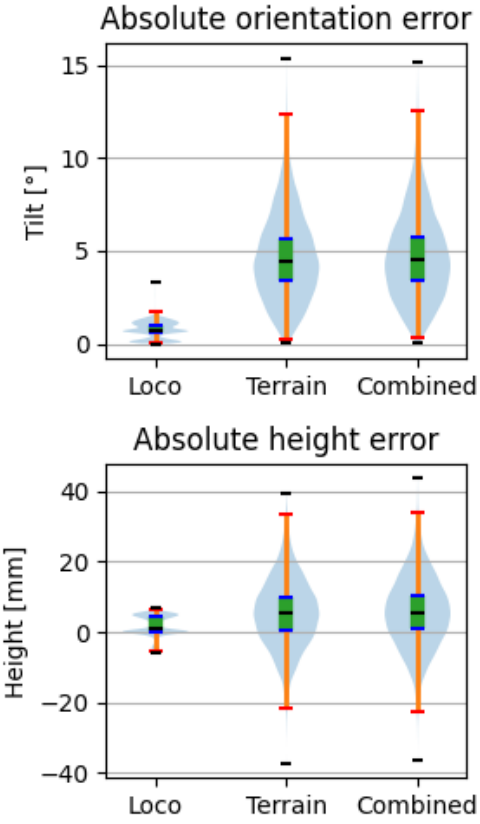

Figure 14: Statistical evaluation of the impact of locomotion error on system accuracy. Violin plots show the error distribution, black marker in the center show the median, blue bars enclose the 31.73 to 68.27 percentile, red bars enclose the 0.27 to 99.73 percentile and the black bars enclose all observed values.

4. Overload Protection

A torque sensor is assembled in each LSS shoulder to detect an overload of the leg drivetrain. This overload can happen e.g. if a small rock gets stuck between leg and chassis of the rover or with specific geometric ground features such as gaps. For this purpose, the torque sensor assembly is not designed for precise torque measurements but rather to detect the overload.

The required torque for the leg drive output is $1.5\,\mathrm{N\,m}$ and for the wheel output $0.5\,\mathrm{N\,m}$. This ensures a save uprighting after impact on Phobos even under difficult circumstances. Since the torque sensor was designed with a measurement range of $\pm 2\,\mathrm{N\,m}$ but an overload range of $\pm 7\,\mathrm{N\,m}$, it has to be equipped with an overload protection to not damage the strain gauges. There are four pins for this purpose, that engage between $1.5\,\mathrm{N\,m}$ and $2.5\,\mathrm{N\,m}$. The exact values depend on the manufacturing tolerances. They are designed as fit bolt with a corresponding oversized whole on the inner ring of the

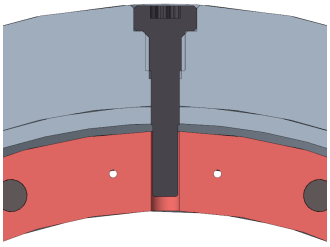

Figure 15: Overload pin design. in the outer ring the fit bolt has a tight tolerance, on the inner ring a designed loose fit.

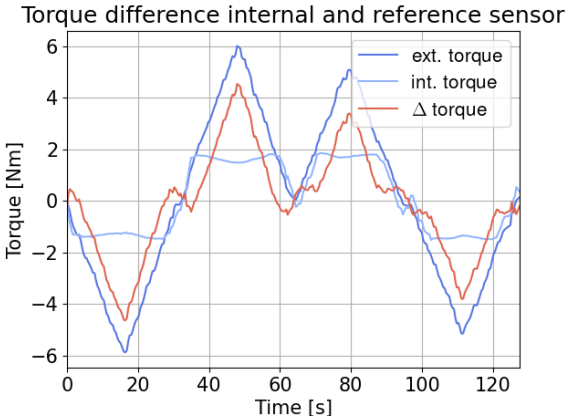

Figure 16: Internal torque sensor reading at -35°C and deviation to the externally measured value

torque sensor. When the inner ring of the sensor, highlighted in red in Figure 15, is deformed, the bolt can move in the oversized hole, but engages when the deformation becomes to big. The oversize diameter value was determined with test and is set to $0.2\,\mathrm{mm}$ in the current configuration.

During the performance test, the locomotion unit was driven with a maximum torque of $6\,\mathrm{N\,m}$ due to required margins. As seen in Figure 16, the pins engage below $2\,\mathrm{N\,m}$ and limit the deformation in the spokes of the torque sensor. This data was recorded during a ramping torque load case, the first negative and positive ramp acting against the movement direction, the last two acting in direction of the movement. It is noticeable that after engagement and during increasing load, the measured torque is dropping slightly. This phenomenon is still under investigation but will be worked around with a suitable threshold that ensures that the decrease has no influence on the blocking detection. Most likely it is caused by the interaction of the pin in its related hole and by the axial load that the crown gear is generating due to the pressure angle of the gearing. Since this is heavily influenced by manufacturing tolerances, the explanation could not yet be confirmed with FEM simulation.

A blockage detection algorithm that additionally considers the motor current measurement is also discussed. Due to the lack of a torque sensor in the wheel drive train, this approach is the only means to protect it against mechanical overloads. Motor current measurements, obtained at the performance tests, are analyzed. Three different load cases are applied to the drive under test: No load, maximum load ($1.25\,\mathrm{N\,m}$) and overload ($2.5\,\mathrm{N\,m}$). Figure 17 shows

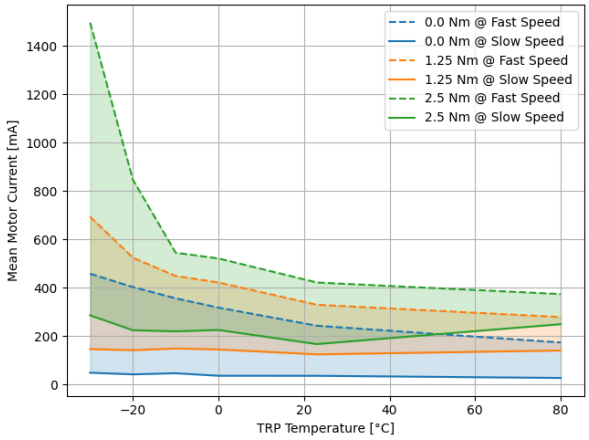

Figure 17: Average Motor current ranges at three different output load cases

the average wheel drive motor current for these three load situations. The shown ranges (colored areas between solid and dashed lines) result from varying the temperature and the motor speed within their respective operational limits. The strong dependency of the motor currents on these two parameters is mainly caused by the lubrication of the harmonic drive gear, where the viscosity is reduced at decreasing temperatures, and the temperature-dependent seal friction. The significant overlapping of the current ranges imply that it would be necessary to calibrate the blockage detection against motor speed and temperature in order to get it robust against false positive blockage detection. Therefore, a current-based blockage detection is not implemented in the current version but might be investigated further as the software development is ongoing.

5. Radiation Monitor

Introduction

The radiation monitor (optical radiation monitor, ORM) is located in the E-Box of the LSS. It is based on an optocoupler and measures the total ionizing dose which is applied to the subsystem based on the degradation of the optical elements. This sensor was already used on the MASCOT lander [10] and proved its concept during the mission.

Temperature compensation

Unfortunately, the sensors response depends on the temperature. This relationship is roughly defined in the data sheet of the component and has to be compensated before the degradation due to radiation can be determined. With a full temperature cycle during the acceptance test campaign, the actual temperature dependency of the output was determined. Figure 18 shows the output voltage of the ORM and the measured temperature during one heat-up. It can clearly be seen that, the measured output voltage changes with changing temperature. The small dent of the output voltage is based on the nonlinear temperature response of the sensor which includes an inflection point. Therefore, the local temperature must be known. This is done by adding a temperature sensor which is placed very close to the ORM. During the mission both values will be measured in parallel.

Since there is no radiation during the TVAC test, the output voltage throughout this test should stay constant. There-

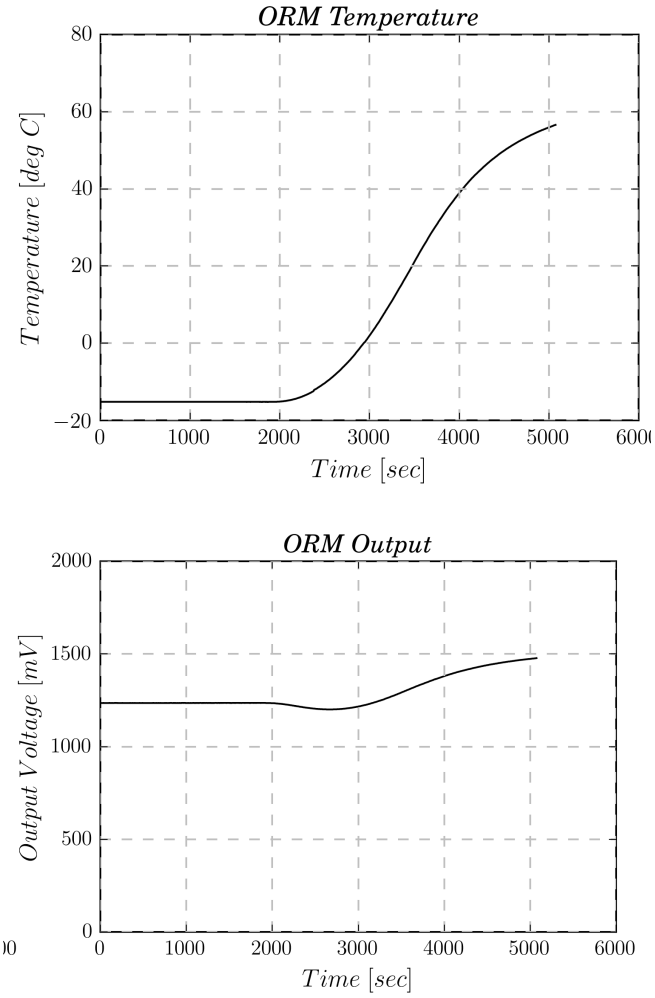

Figure 18: ORM Output voltage over time in comparison to the measured temperature.

fore, the correction factor can be computed by dividing the expected voltage by the currently measured voltage at each measurement point. These values can then be saved and used in a linear interpolation lookup table or a polynomial fit can be made to compute the correction factor as a function of the current temperature. The corrected voltage then results as the product of correction factor and uncorrected measured voltage.

Measurement of radiation

Once the optical elements of the ORM degrade by the applied total ionizing dose, the output voltage will change respectively. The difference between the temperature compensated voltage at the beginning of the mission and the actual temperature compensated voltage will provide the radiation information with the linear relationship $1\,\mathrm{mV\,Gy^{-1}}$.

6. SOFTWARE

The LSS's software, called LOCO-SW, uses the E-Box housekeeping data in order to monitor the system on-board and recover it autonomously whenever possible. Residuals serving for fault detection are parameters that can still be changed during the ongoing mission. Nevertheless, reliable initial values have to be found during the characterization of the system. Among them are parameters for blockage detection or a successful health check, which are presented in previous sections.

Table 3: Content of the housekeeping packet containing the direct kinematics and system state.

Label	Description
Current timestamp	Current time
Start timestamp	Time at the beginning of a command
Driven distance	[m] Relatively driven distance since start timestamp
Driven yaw angle	[rad] Relatively driven yaw angle since start timestamp
Orientation X	X-component of the orientation vector
Orientation Y	Y-component of the orientation vector
Orientation Z	Z-component of the orientation vector
Height	[m] Height of the rover
Motor blockage	Indicates a blockage at leg/wheel
System state	Flags to indicate the system state
System condition	Flags to indicate the system conditions
Leg angle FL	[mrad] Actual leg angle front left
Leg angle RL	[mrad] Actual leg angle rear left
Leg angle RR	[mrad] Actual leg angle rear right
Leg angle FR	[mrad] Actual leg angle front right

The housekeeping data from the E-Box, which are around 800 bytes per instance, are sent with a frequency of 10Hz to the LOCO-SW. If they were sent to ground in the same frequency and size, the data traffic would exceed the mission's capacities. Thus, data has to be carefully selected. In particular, the information about a successful or failed health check is sent to ground with 24 bytes of additional data specifying what has happened during this check. They are used to send the occurred failure ID for the concerned motor plus further relevant information to obtain the system state. The same happens for the self-check that the software is running on the system each time after a startup.

LSS state & Rover Kinematics

The LSS is the only subsystem in IDEFIX that has knowledge about the rotational wheel and leg position and thereby the rover pose. This is important on-board information (see Table 3) for other subsystems: the navigation benefits from the wheel odometry and the sun alignment needs knowledge about the rover pose. The driven distance and yaw angle serve as wheel odometry for operation purposes and the navigation subsystem, combined with the given time stamps. The orientation and height, which are both calculated relative to a reference plane, assist the sun alignment to have additional knowledge about the rover positioning. The motor blockage, system state and system condition are flags that indicate the status of the LSS to inform what the LSS is currently able to perform. For the characterization of the LSS, it is very important to tune the FDIR algorithms within the LOCO-SW properly so that these flags are reliable. Finally, the leg angles inform about the current leg positioning, e.g. to know if the single legs reached their target position during the uprighting sequence.

In order to validate these direct kinematic calculations, tests were performed on a prototype rover and in simulation [8][11]. They showed that the rover height and orientation relatively to a reference plane are very reliable. So is the driven relative distance since the start of a command, not con-

sidering the wheel slip in the widely unknown environment of Phobos.

7. Conclusion

The extensive test campaign for the qualification and acceptance of the LSS resulted in a lot of data, which can be used beyond the pure qualification of the subsystem. Different analyses of these data logs were performed after the qualification and enriched by additional simulation. In this paper, we gave an overview of the data that has been collected and presented some of the most interesting analysis results. These analyses are a very important building block for the parameterization of the LSS software that is partly done now and will be updated during the cruise phase and on Phobos. For upcoming health checks and the extensive check-out of the LSS, once IDEFIX has landed on Phobos, this characterization of the LSS provides a solid reference of the LSS as it was before launch.

References

[1] S. Ulamec, P. Michel *et al.*, "A rover for the JAXA MMX Mission to Phobos," in *Proceedings of the International Austronautical Congress (IAC)*, 2019.

[2] J. Bertrand, S. Tardivel *et al.*, "Roving on Phobos: Challenges of the MMX Rover for Space Robotics," in *Proceedings of the 15th Symposium on Advanced Space Technologies in Robotics and Automation (ASTRA)*, 2019.

[3] S. Ulamec, P. Michel *et al.*, "Scientific Objectives of the MMX Rover Mission to Phobos," in *Proceedings of the Global Space Exploration Conference (GLEX)*, 2021.

[4] H.-J. Sedlmayr, S. Barthelmes *et al.*, "MMX – Development of a Rover Locomotion System for Phobos," in *Proceedings of the IEEE Aerospace Conference*, 2020.

[5] S. Barthelmes, T. Bahls *et al.*, "MMX Rover Locomotion Subsystem - Development and Testing towards the Flight Model," in *Proceedings of the IEEE Aerospace Conference*, 2022.

[6] V. Langofer, R. Bayer, and A. Kolb, "MMX Locomotion Subsystem: mechanics for extraterrestrial low gravity drive," in *Proceedings of the IEEE Aerospace Conference*, 2023.

[7] S. Barthelmes, R. Bayer *et al.*, "qualification of the mmx rover locomotion subsystem for the martian moon phobos," in *Proceedings of the IEEE Aerospace Conference*, 2023.

[8] J. Skibbe, S. Barthelmes, and F. Buse, "Locomotion Control Functions for the Active Chassis of the MMX Rover," in *Proceedings of the IEEE Aerospace Conference*, 2021.

[9] J. Skibbe, E. Aitier *et al.*, "Fault detection, isolation and recovery in the mmx rover locomotion subsystem," in *2023 IEEE Aerospace Conference*, 2023.

[10] J. Reill, H.-J. Sedlmayr *et al.*, "MASCOT – Asteroid Lander with Innovative Mobility Mechanism," in *13th Symposium on Advanced Space Technologies in Robotics and Automation (ASTRA)*, 2015.

[11] F. Buse, A. Pignède *et al.*, "MMX Rover Simulation - Robotic Simulations for Phobos Operations," in *2022 IEEE Aerospace Conference*, 2022.

Biography

Stefan Barthelmes *received his Dr.-Ing. degree in Electrical Engineering at TU Darmstadt and his B.Sc. and M.Sc. degree in Mechanical Engineering from TU München. He is currently working as a researcher at the Institute of System Dynamics and Control of the German Aerospace Center (DLR). His main research focus is model-based chassis control and simulation model development of planetary exploration rovers. Within the MMX mission, he is responsible for the rover's locomotion subsystem.*

Fabian Buse *received his Dr.-Ing. degree in Aerospace Engineering from Tōhoku University and his B. Sc. and M. Sc. from RWTH Aachen University. Since 2015, he has been Research Associate at the Institute of System Dynamics and Control (SR). His research interests are in terramechanics for planetary rovers. He is the lead engineer of the DLR Terramechanics Robotic Locomotion Lab (TROLL) and is leading the rover simulation for the MMX Rover project.*

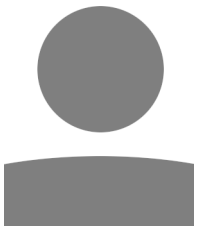

Maxime Chalon *received his Dr.-Ing. degree in Control Theory at Mines ParisTech and his B.Sc. and M.Sc. degree in Mechatronics Engineering from Ecole des Mines d'Ales. He is currently working as a research associate at the Institute of Robotics and Mechatronics of the German Aerospace Center (DLR). His main research focus is space robotics. Within the MMX mission, he is responsible for the rover's system engineering and partially the locomotion system engineering.*

Bastian Deutschmann *received his Dr.-Ing. degree in Robotics and Mechatronics at Leibniz University of Hannover and his Dipl.-Ing. degree in Mechanical Engineering from University of Stuttgart. He is currently working as a senior research scientist at the Institute of Robotics and Mechatronics of the German Aerospace Center (DLR). His main research focus is terrestrial and space robotics. Within the MMX mission, he is co-responsible for the rover's system engineering.*

André Fonseca Prince *received his MSc. degree in Mechatronics Engineering from the Politecnico di Torino, Italy in 2020. Since then, he has been working in the Robotics and Mechatronics Institute at the German Aerospace Center (DLR) as Mechatronics engineer. He has contributed to the Power Management and Data Handling systems of the Moon analogue multi-robot project ARCHES since 2020 and, within MMX, to the firmware in the central electronic box of the rover's locomotion subsystem. His fields*

of interest are electronics communication, motor control, and power electronics within robotic planetary exploration.

Franz Hacker *received his Dipl.-Ing. degree in Electrical Engineering and Information Technology from TU München. Since 1994, he works as research associate at the German Aerospace Center, Institute of Robotics and Mechatronics. His main research focus is the design and optimization of analog electronics and sensors used for robotic systems in terrestrial and space applications. Within the MMX mission, he is responsible for the central electronic box of the rover's locomotion subsystem.*

Roman Holderried *received his B.Eng. from University of Applied Science in Kempten and his M.Sc. from University of Applied Science Munich, both in Electrical Engineering. Since 2019, he has been with the German Aerospace Center, Institute of Robotics and Mechatronics. His main research interest is the design and implementation of control algorithms for electrical drives in terrestrial and space robotics applications. Within the MMX project, he contributed to the development of the drive controllers of the locomotion subsystem and was involved in the test design of the qualification test campaign.*

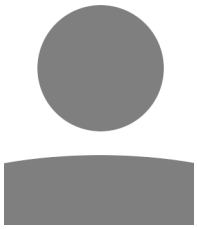

Alexander Kolb *graduated as a Dipl.-Ing. in Mechatronics from the University of Innsbruck, Austria in 2019. Since then, he has been working at the German Aerospace Center (DLR), Institute of Robotics and Mechatronics as a mechanical engineer. He did his first work in the field of medical robotics, transitioning to space domain in 2020. His research focus lies on the optimization of electromechanical actuators.*

Viktor Langofer *received the degrees of B.Sc. and M.Sc. from Technische Universität Kaiserslautern. Since 2017, he has been Research Associate at the German Aerospace Center (DLR), Institute of Robotics and Mechatronics. His main area of activities are research in compliant and tendondriven mechanisms in humanoid robotics, as well actuators design for space applications. He is responsible for the mechanical design of the locomotion subsystem of the MMX Rover.*

Hans-Juergen Sedlmayr *received his Dipl.-Ing. degree in Electrical Engineering from the University of Applied Science Munich in 1992. Since 2001, he has been with the German Aerospace Center, Institute of Robotics and Mechatronics. His main research focus is in the field of radiation testing of electric and electronics parts and embedded software development inside robots for terrestrial and space applications. Within the MMX mission, he is responsible for quality assurance of the rover's locomotion subsystem.*

Juliane Skibbe *studied Mathematics at the University of Wuerzburg and the Université d'Orléans. After finishing her Master's degree in 2018, she started working as a research associate at the Institute of System Dynamics and Control of the German Aerospace Center (DLR). Today, she leads the MMX Locomotion Software team. Her main research focus is on developing locomotion control algorithms for rover for planetary exploration, in particular fault detection, isolation and recovery.*

Bernhard Vodermayer *received his degree computer science in 2006 at the Technical University of Munich while he has been scientifically associated with the Institute of Robotics and Mechatronics since 2004. Till 2012, he played a major key role in the development and the technology transfer of the DLR's left ventricular heart assist device DLR-LVAS. Since 2010, he is scientifically related to space based technologies for safe robotic docking and energy management of wheeled, autonomous vehicles for planetary exploration. His research interests are in the field of novel, future emerging technology based actuator and sensor systems, polymer-based systems and related production processes, space technologies, biomedical devices and active implants. Within MMX he is responsible for the development and qualification of the rotational sensors used in the Locomotion subsystem.*